Vol 17 No 6, June 2008
1674-1056/2008/17(06)/2072-06

Chinese Physics B

© 2008 Chin. Phys. Soc.
and IOP Publishing Ltd

Use of photoelectron laser phase determination method for attosecond measurements with quantum-mechanical calculations

Ge Yu-Cheng(葛愉成)†

Department of Technical Physics and DOE Key Laboratory of Heavy Ion Physics, Peking University, Beijing 100871, *China*

(Received 2 August 2007; revised manuscript received 8 October 2007)

This paper calculates quantum-mechanically the photoelectron energy spectra excited by attosecond x-rays in the presence of a few-cycle laser. A photoelectron laser phase determination method is used for precise measurements of the pulse natural properties of x-ray intensity and the instantaneous frequency profiles. As a direct procedure without any previous pulse profile assumptions and time-resolved measurements as well as data fitting analysis, this method can be used to improve the time resolutions of attosecond timing and measurements with metrological precision. The measurement range is half of a laser optical cycle.

Keywords: attosecond measurement, photoelectron spectrum, laser phase determination, transfer equation

PACC: 3365, 3280F, 3280, 3365C

1. Introduction

With the development of state-of-the-art ultrashort laser systems, high-order harmonic generation (HHG) has been an effective way to produce attosecond extreme ultra-violet (XUV) and x-ray pulses. In this research area, many Chinese authors have reported their results of studying the atomic ionization in a strong laser field and the dynamic mechanism of HHG.[1−8] Different from the XUV pulses, attosecond x-rays particularly in the water-window ($283.7 - 532.1$ eV) have their own advantages in ultrafast chemical reaction researches.[9] Today, producing and measuring such attosecond x-rays is a subject attracting increasing attention.

The natural properties of an x-ray pulse include temporal distributions of intensity and the instantaneous frequency. They may be complicated due to x-ray generation mechanism, transports and interactions with media. So far, several methods have been developed to measure the pulse durations of attosecond XUVs.[10−22] However, most of them use previous pulse assumptions and data fitting analysis with time-resolved measurements of photoelectron spectra. In fact, reconstructing the natural properties of an attosecond x-ray with metrological precisions from non-time-resolved measurement data still remains a challenge, but such measured properties are useful for fast online pulse evaluation and improvement.

Seeking new methods to measure atto- and femtosecond x-ray pulses, we proposed transfer equations and photoelectron laser phase determination methods.[23−27] With these transfer equations and methods, the birth time of each photoelectron measured in a cross correlation experiment between an attosecond x-ray and a few-cycle dressing laser [10−13] can be determined, and the detailed x-ray pulse information can be reconstructed directly from a measured photoelectron energy spectrum (PES). However, these works were based on semi-classical calculations.

In this paper, the quantum-mechanically calculated PESs are compared with their classical predictions. We use the photoelectron laser phase determination method to reconstruct both the intensity and the instantaneous frequency profiles of attosecond x-rays from quantum–mechanically calculated PESs. The results show how the quantum effect of photoionization plays a role in determining the photoelectron laser phase, and that the method works on high precisions with high energy attosecond x-rays.

†E-mail: gyc@pku.edu.cn

2. Strong field approximation

The electron motion satisfies the time-dependent Shrödinger equation in atomic units:

$$\mathrm{i}\frac{\partial}{\partial t}\Psi(\boldsymbol{r},t)=\left[-\frac{1}{2}\nabla^2-\frac{1}{r}-\boldsymbol{r}E(t)\right]\Psi(\boldsymbol{r},t), \quad (1)$$

where $\boldsymbol{r}=(x,y,z)$ denotes the space coordinates, and $\Psi(\boldsymbol{r},t)$ represents the electron wavefunction. The electric field $\boldsymbol{E}(t)=\boldsymbol{E}_{\mathrm{L}}(t)+\boldsymbol{E}_{\mathrm{X}}(t)$ comprises the contribution of a linearly polarized laser, $\boldsymbol{E}_{\mathrm{L}}(t)=E_0F(t)\cos(\omega_{\mathrm{L}}t+\Phi)$ (x direction, Φ is the carrier-envelope phase), and an x-ray, $\boldsymbol{E}_{\mathrm{X}}(t)=E_{\mathrm{X}}\cos(\omega_{\mathrm{X}}t)$ (x direction). $F(t)$ is the laser field (maximum of E_0) envelope shape peaked at $t=0$. ω_{L} and ω_{X} are laser and x-ray angular frequencies, respectively. The electric field is related to the vector potential $\boldsymbol{A}(t)$ by $\boldsymbol{E}(t)=-(1/c)\partial_t\boldsymbol{A}(t)$, where c is the velocity of light.

Equation (1) can be solved analytically by applying the strong field approximation (SFA).[28,29] As a result, the Coulomb continuum eigenfunctions may be substituted by plane waves, and Eq.(1) is integrated by using the expression $\Psi(\boldsymbol{r},t)=\mathrm{e}^{\mathrm{i}I_{\mathrm{p}}t}\left(|0\rangle+\int\mathrm{d}^3\boldsymbol{p}b(\boldsymbol{p},t)|\boldsymbol{p}\rangle\right)$. Here $|0\rangle$ denotes the atomic ground state with ionization potential I_{p}. The plane wave is given by $|\boldsymbol{p}\rangle=\exp(\mathrm{i}\boldsymbol{p}\cdot\boldsymbol{r})$, in which $\boldsymbol{p}$ is the canonical momentum of electron, $\boldsymbol{p}=\boldsymbol{v}+\boldsymbol{A}(t)$, and $\boldsymbol{v}$ is the velocity of electron. $b(\boldsymbol{p},t)$ is the momentum space wavefunction of free electrons. Within the SFA, the probability amplitude for transition from $|0\rangle$ to a final state $|\boldsymbol{p}\rangle$ is

$$b(\boldsymbol{p})=\mathrm{i}\int_{-\infty}^{\infty}\mathrm{d}tE(t)d_x[\boldsymbol{p}-\boldsymbol{A}(t)]\mathrm{e}^{-\mathrm{i}\widetilde{S}(t)}, \quad (2)$$

where $\widetilde{S}(t)$ is defined as the quasiclassical action,

$$\widetilde{S}(t)=\int_t^{\infty}\mathrm{d}t'\left\{\frac{[\boldsymbol{p}-\boldsymbol{A}(t')]^2}{2}+I_{\mathrm{p}}\right\}. \quad (3)$$

Here, $\boldsymbol{d}(\boldsymbol{p})=\langle\boldsymbol{p}|\boldsymbol{x}|0\rangle$ is the atomic dipole matrix element for the bound-free transition, and $d_x(\boldsymbol{p})$ is the component parallel to the polarization axis. $d_x(\boldsymbol{p})=\mathrm{i}2^{7/2}\alpha^{5/4}\boldsymbol{p}/\pi(2I_{\mathrm{p}}+p^2)^3$ for the hydrogen bound s state ($\alpha=2I_{\mathrm{p}}$, $I_{\mathrm{p}}=13.6\,\mathrm{eV}$).

The PES is given by $|b(\boldsymbol{p})|^2$. For simplicity, a linearly polarized laser with the wavelength $\lambda_{\mathrm{L}}=750\,\mathrm{nm}$ and $\Phi=0^\circ$ is used in schematic calculations. $F(t)=\exp[-4ln2\cdot(t)^2/\tau_{\mathrm{L}}^2]$ is a Gaussian function with the pulse duration $\tau_{\mathrm{L}}=7$ fs in full width at half maximum (FWHM). As shown in Fig.1(a), a $\tau_{\mathrm{X}}=0.2$ fs (pulse duration in FWHM) Gaussian shape x-ray pulse is temporally centred at $t=0.31\,\mathrm{fs}$, being cross-correlated to the laser phases 0–$\pi/2$, or 0–0.625 fs in time domain. The initial x-ray intensity profile is denoted as $f_0(t)$. In fact, the x-ray pulse can be temporally located within half laser optical cycle (phases $-\pi/2$–$\pi/2$). The instantaneous frequency profile is assumed to be a simple function, $W_{\mathrm{i}}(t)$, peaked at ω_0.

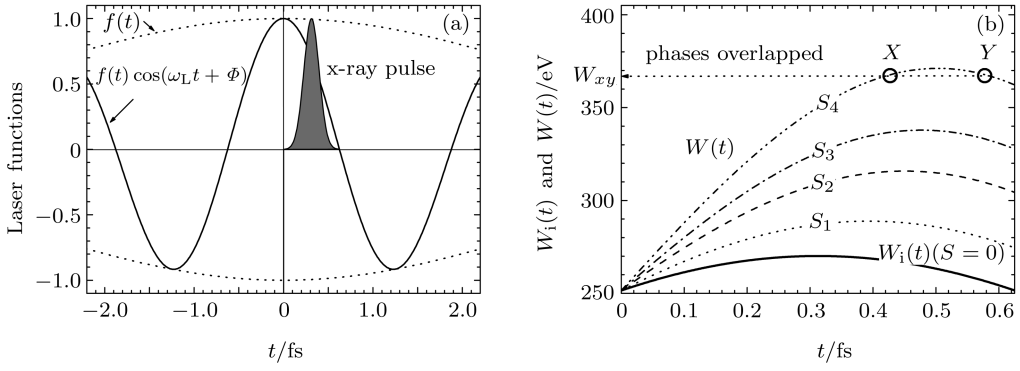


Fig.1. (a) An illustration of cross correlation between laser and x-ray pulses. The solid and dotted lines are laser field and its envelope, respectively. (b) The photoelectron final energy, $W(t)$, vs birth time t, modulated with different intensity lasers, $S_{1-4}=(0.5,2.5,5,10)\times10^{13}\,\mathrm{W/cm^2}$.

3. Transfer equations and photoelectron laser phase determination method

From the classical point of view,[26] the final photoelectron velocity $v(t)$ at $\theta=0^\circ$ and 180° with respect to the laser polarization can be written as

$$v(t)=v_{\mathrm{i}}(t)\pm2\sqrt{\frac{U_0}{m_{\mathrm{e}}}}F(t)\sin(\omega_{\mathrm{L}}t+\Phi), \quad (4)$$

where m_{e} and $U_0=E_0^2/4m_{\mathrm{e}}\omega_{\mathrm{L}}^2$ are the electron mass and the ponderomotive energy at $t=0$, respectively. Here, t denotes the photoelectron birth time.

The choice of the sign in front of the square root of Eq.(4) depends on $\theta = 0^\circ$ (+) or 180° (−). $v_\mathrm{i}(t) = \sqrt{2W_\mathrm{i}(t)/m_\mathrm{e}} = \sqrt{2[\omega_\mathrm{i}(t) - I_\mathrm{p}]/m_\mathrm{e}}$ is the initial velocity of a photoelectron born at t. $W_\mathrm{i}(t)$ is the corresponding photoelectron initial energy. Its final energy is $W(t) = m_\mathrm{e}v^2(t)/2$. $v(0) = v_\mathrm{i}(0)$ means that no momentum shift is finally experienced by a photoelectron burn at $t = 0$. Therefore, we can experimentally adjust the x-ray pulse start ($\theta = 0^\circ$ measurement) or end ($\theta = 180^\circ$ measurement) to $t = 0$ by keeping the low end of PES invariable. Figure 1(b) shows the photoelectron final energies as functions of the birth time (t), $W(t)$, which are calculated at $\theta = 0^\circ$ with different laser intensities, $S_{1-4} = (0.5, 2.5, 5, 10) \times 10^{13}\,\mathrm{W/cm^2}$.

The phase overlapping makes PES complicated. In the absence of the laser, the measured PES is a sum of photoelectrons generated at different times. This means that each spectral position corresponds to two different birth times for current $\omega_\mathrm{i}(t)$ at $S = 0$. We call it complete phase-overlapping. As the laser intensity increases, the line of $W_\mathrm{i}(t)$ is raised from one end in time domain. With a higher laser intensity (e.g., S_4 in Fig.1(b)), most phase-overlapping vanish, only a small portion of the PES contains phase-overlapping. For example, circles X and Y in Fig.1(b) point to the same energy of W_{xy} where phase-overlapping occurs. In order to avoid the phase-overlapping and obtain a continuously increasing line of $W(t)$, $\mathrm{d}v(t)/\mathrm{d}t > 0$, i.e., $\sqrt{U_0} > [-\sqrt{m_\mathrm{e}}\mathrm{d}v_\mathrm{i}(t)/\mathrm{d}t]/[2\omega_\mathrm{L}\cos(\omega_\mathrm{L}t + \Phi)]$, is required. However, the laser-induced part of the above threshold ionization (ATI) spectrum limits the laser intensity to be increased to very high level.[18,30] According to the simple condition,[18] $8U_0 \leq \omega_\mathrm{i}(t) - I_\mathrm{p}$, the moderate laser intensity $S_4 = 10 \times 10^{13}\,\mathrm{W/cm^2}$ ($U_0 = 5.25\,\mathrm{eV}$) and less ensure that the PESs are fully separated from the ATI spectra for x-ray frequencies concerned.

For a photoelectron moving at $\theta = 0^\circ$, we define $W_{0^\circ}^\mathrm{L}$ ($W_{0^\circ}^\mathrm{H}$) as the final energy measured with low (high) laser intensity, S_L (S_H) (or low (high) ponderomotive energy U_0^L (U_0^H)). According to Ref.[26], we have the following equations to calculate photoelectron birth time t and initial kinetic energy $W_\mathrm{i}(t)$,

$$F(t)\sin(\omega_\mathrm{L}t + \Phi) = \frac{\sqrt{W_{0^\circ}^\mathrm{H}} - \sqrt{W_{0^\circ}^\mathrm{L}}}{\sqrt{2U_0^\mathrm{H}} - \sqrt{2U_0^\mathrm{L}}},$$
$$W_\mathrm{i}(t) = \left[\sqrt{W_{0^\circ}^\mathrm{H}} - \sqrt{2U_0^\mathrm{H}} \cdot \frac{\sqrt{W_{0^\circ}^\mathrm{H}} - \sqrt{W_{0^\circ}^\mathrm{L}}}{\sqrt{2U_0^\mathrm{H}} - \sqrt{2U_0^\mathrm{L}}}\right]^2. \quad (5)$$

Similarly, for a photoelectron moving at $\theta = 180^\circ$,

$$F(t)\sin(\omega_\mathrm{L}t + \Phi) = -\frac{\sqrt{W_{180^\circ}^\mathrm{H}} - \sqrt{W_{180^\circ}^\mathrm{L}}}{\sqrt{2U_0^\mathrm{H}} - \sqrt{2U_0^\mathrm{L}}},$$
$$W_\mathrm{i}(t) = \left[\sqrt{W_{180^\circ}^\mathrm{H}} - \sqrt{2U_0^\mathrm{H}} \times \frac{\sqrt{W_{180^\circ}^\mathrm{H}} - \sqrt{W_{180^\circ}^\mathrm{L}}}{\sqrt{2U_0^\mathrm{H}} - \sqrt{2U_0^\mathrm{L}}}\right]^2, \quad (6)$$

where $W_{180^\circ}^\mathrm{L}$ ($W_{180^\circ}^\mathrm{H}$) denotes the photoelectron final energy measured with laser intensity S_L (S_H). Equations (5) and (6) are basic equations. The key problem is how to determine the energies $W_{0^\circ}^\mathrm{L}$ and $W_{0^\circ}^\mathrm{H}$ (or $W_{180^\circ}^\mathrm{L}$ and $W_{180^\circ}^\mathrm{H}$) which correspond to the same laser phase.

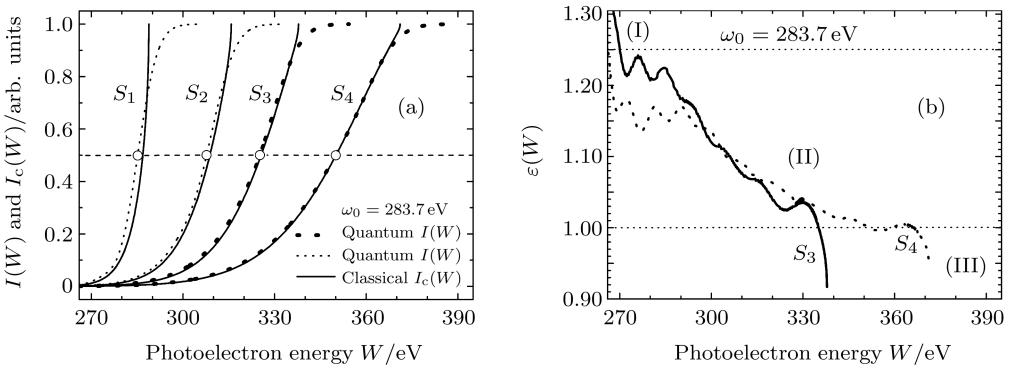


Fig.2. (a) Quantum-mechanically calculated integral terms of PESs (thin and thick dotted lines), $I(W)$, and classical predictions (solid lines), $I_\mathrm{c}(W)$, with $\omega_0 = 283.7\,\mathrm{eV}$ and different laser intensities, $S_{1-4} = (0.5, 2.5, 5, 10) \times 10^{13}\,\mathrm{W/cm^2}$. (b) $\epsilon(W)$ vs photoelectron energy W for different laser intensities, $S_{3,4}$. Here, $\varepsilon(W) = I(W)/I_\mathrm{c}(W)$. (I)–(III) denote three stages of $\epsilon(W)$.

The PES, $n(W)$, is defined as the number of photoelectrons per unit energy. For an initial x-ray intensity profile $f_0(t)$, the number of photoelectrons measured from energy $W_1 = W_{\min}$ (the low end of the PES) to W is proportional to the number of x-ray photons irradiated from the instant $t_1 = t_s$ to t,[26]

$$\int_{t_s}^{t} f_0(t_1)\mathrm{d}t_1 = \mu \int_{W_{\min}}^{W} n(W_1)\mathrm{d}W_1 \equiv \mu I(W), \tag{7}$$

where μ is a constant. The integral of the left-hand side of Eq.(7) is related only to time t, while the corresponding spectral position W is variable (if $t \neq 0$) when the laser intensity changes (see circle points in Fig.2(a)). Therefore, Eq.(7) can be used to determine the photoelectron energies $W^{\mathrm{L}}_{0^\circ}$ and $W^{\mathrm{H}}_{0^\circ}$ (or $W^{\mathrm{L}}_{180^\circ}$ and $W^{\mathrm{H}}_{180^\circ}$) from the integral terms of two PESs, $I(W)$, measured with two laser intensities, S_{L} and S_{H}. After solving t for each spectral position W from the first equation of Eq.(5) or Eq.(6), the initial photoelectron energy $W_{\mathrm{i}}(t)$ can be calculated using the second equation. The x-ray pulse intensity and the instantaneous frequency are $f(t) = \mu \mathrm{d}I(W)/\mathrm{d}t$ and $\omega_{\mathrm{i}}(t) = W_{\mathrm{i}}(t) + I_{\mathrm{P}}$, respectively.

4. Calculations

Figure 2(a) shows the normalized $I(W)$ (thin and thick dotted lines) quantum-mechanically calculated with $\omega_0 = 283.7\,\mathrm{eV}$ and different laser intensities, $S_{1-4} = (0.5, 2.5, 5, 10) \times 10^{13}$, and their classical predictions, $I_{\mathrm{c}}(W)$ (solid lines). As plots show, the differences between $I(W)$ and $I_{\mathrm{c}}(W)$ are small. These tolerable differences gave clues of deriving the transfer equations from the classical point of view,[26] and ensure the use of these equations for attosecond measurements. At low laser intensities, the differences between $I(W)$ and $I_{\mathrm{c}}(W)$ are obvious. In the quantum view, the enhancement of photo-ionization reflects the quantum interferences between electron wave packets generated at different times. As the laser intensity increases, the quantum results get close to the classical predictions. We can define a quantum enhancement factor, $\varepsilon(W) \equiv I(W)/I_{\mathrm{c}}(W)$. Figure 2(b) shows $\varepsilon(W)$ with different laser intensities, $S_{3,4} = (5, 10) \times 10^{13}\,\mathrm{W/cm^2}$.

Obviously, each line of $\varepsilon(W)$ can be divided into three stages. In the middle stage (II) (see Fig.2(b)), $\varepsilon(W) \approx 1$, the method gives good pulse reconstructions (Fig.3). The quantum enhancement will result in a small time correction δ_1 for x-ray frequency profile and δ_2 for intensity. Therefore, the final results of $\omega_{\mathrm{i}}(t)$ and $f(t)$ should be temporally shifted from the initially derived data by $-\delta_1$ and $-\delta_2$, respectively. In the first stage (I) at low W, $\varepsilon(W) > 1$, even $\varepsilon(W) \gg 1$, the quantum enhancements are much larger than the classical predictions. Since the values of $f_0(t)$ are small there, the phase determination method still works well. In the third stage (III) at high W, $I(W)$ is notably deviated from $I_{\mathrm{c}}(W)$ due to quantum effect.

The dotted lines in Figs.3(a) and 3(b) are $\omega_{\mathrm{i}}(t)$ and $f(t)$ retrieved from the PESs calculated at $\theta = 0^\circ$ with $\omega_0 = 283.7\,\mathrm{eV}$, $S_{\mathrm{L}} = 2.5 \times 10^{13}\,\mathrm{W/cm^2}$ and $S_{\mathrm{H}} = 10 \times 10^{13}\,\mathrm{W/cm^2}$. $\delta_1 = +0.030\,\mathrm{fs}$ and $\delta_2 = +0.020\,\mathrm{fs}$ are very small. Experimentally, δ_1 can be determined by extending and temporally shifting the initially derived $W_{\mathrm{i}}(t')$ to meet the energy position of the low end of PES measured in the absence of the laser. Approximately, $\delta_2 \approx \delta_1$. For $\theta = 0^\circ$ calculations, only the rising-sides of $\omega_{\mathrm{i}}(t)$ and $f(t)$ are successfully reconstructed. The badly retrieved data of the falling-sides of $\omega_{\mathrm{i}}(t)$ and $f(t)$ reflect the phase overlapping. To solve this problem, we temporally adjust the pulse end to $t = 0$ and calculate PESs at $\theta = 180^\circ$ (or at $\theta = 0^\circ$ with a $\Phi = 180^\circ$ laser field) with the same laser intensities S_{L} and S_{H}, the falling-sides of $\omega_i(t)$ and $f(t)$ are successfully reconstructed, shown as dashed lines in Figs.3(a) and 3(b). Except for the data with large deviations from the initial profiles, the combination of the data calculated at $\theta = 0^\circ$ and 180° gives successful pulse reconstructions of intensity and the instantaneous frequency profiles (see open circles in Figs.3(a) and 3(b)).

Figures 3(c) and 3(d) show successful pulse reconstructions by combining the data calculated at $\theta = 0^\circ$ and 180° with $\omega_0 = 283.7\,\mathrm{eV}$, $S_{\mathrm{L}} = 5 \times 10^{13}\,\mathrm{W/cm^2}$ and $S_{\mathrm{H}} = 10 \times 10^{13}\,\mathrm{W/cm^2}$, while Figs.3(e) and 3(f) give similar successful pulse reconstructions with $\omega_0 = 532.1\,\mathrm{eV}$. Calculations with $S_{\mathrm{H}} = (20 - 40) \times 10^{13}\,\mathrm{W/cm^2}$ give better pulse reconstructions because of less phase overlapping for current frequency profile.

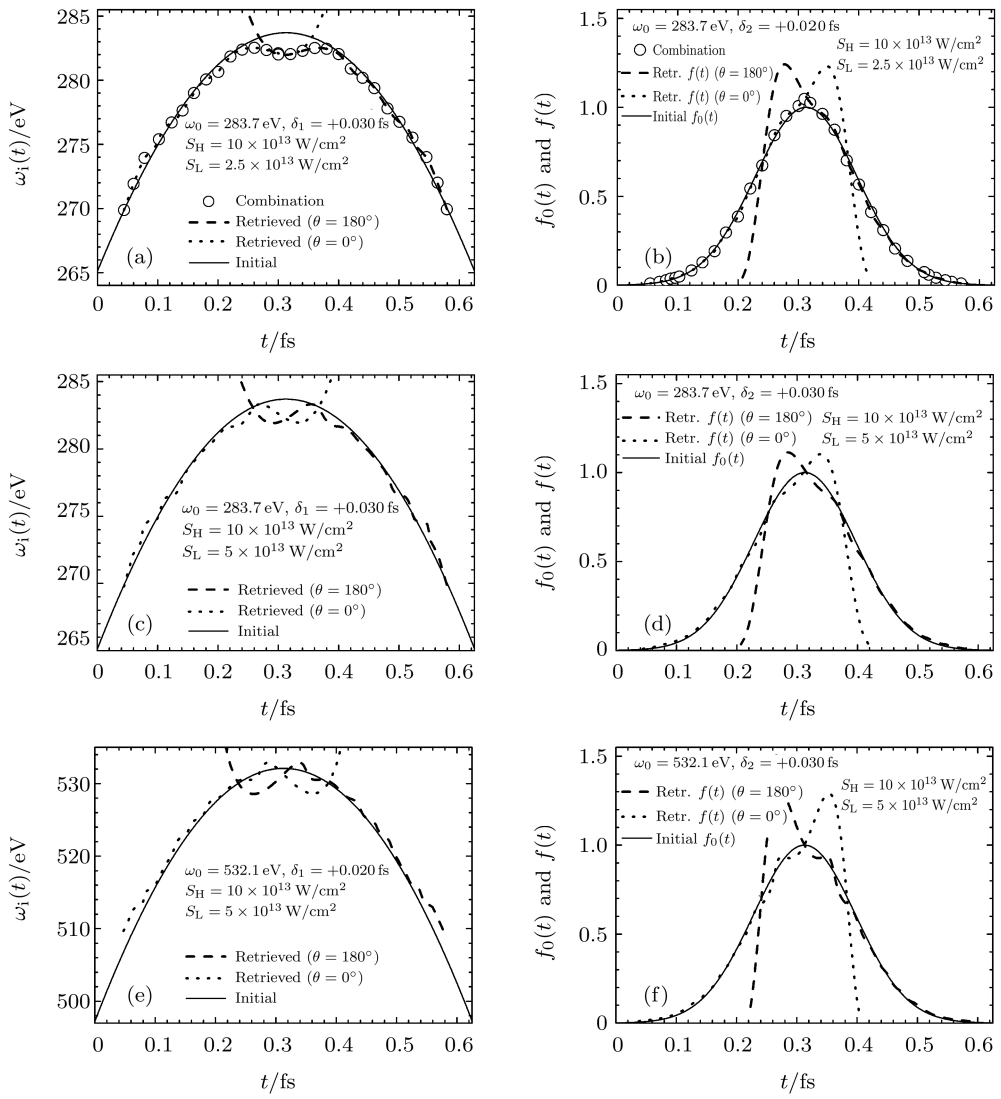


Fig.3. Pulse reconstructions with $\omega_0 = 283.7\,\mathrm{eV}$ (a-d) and $\omega_0 = 532.1\,\mathrm{eV}$ (e,f). (a,b) $S_L = 2.5 \times 10^{13}\,\mathrm{W/cm^2}$, $S_H = 10 \times 10^{13}\,\mathrm{W/cm^2}$. (c-f) $S_L = 5 \times 10^{13}\,\mathrm{W/cm^2}$, $S_H = 10 \times 10^{13}\,\mathrm{W/cm^2}$. Solid lines in (a,c,e) are the x-ray frequency profile, $\omega_i(t)$. Solid lines in (b,d,f) are the initial x-ray intensity profile, $f_0(t)$. Dotted lines are $\omega_i(t)$ and $f(t)$ retrieved from the PESs calculated at $\theta = 0°$. Dashed lines are $\omega_i(t)$ and $f(t)$ retrieved at $\theta = 180°$. Circles in (a,b) represent the pulse profiles reconstructed by combining the data retrieved at $\theta = 0°$ and 180°, which are almost the same as initial ones.

5. Summary

The transfer equations and the photoelectron laser phase determination method can be used to measure high energy attosecond x-rays with high precisions. The quantum effect of photo-ionization results in a temporal shift in determining the birth time of a photoelectron. The rising sides of x-ray intensity and the instantaneous frequency profiles can be directly reconstructed from two PESs measured at $\theta = 0°$. The falling sides can be reconstructed from two PESs measured at $\theta = 180°$ (or $\theta = 0°$ and $\Phi = 180°$). The combination of these retrieved data can give successful pulse reconstructions. Wide calculations show that this method is capable of getting detailed pulse information, including possible asymmetries of frequency and intensity profiles.

Acknowledgments

We acknowledge the assistance of Haiping He, and discussions with Professor K. Burnett at Oxford University, M. Lewenstein at the Institut de Ciencies Fotoniques, D. X. Jiang, Y. L. Ye, J. X. Chen and H. T. Liu at Peking University.

References

[1] Wang Z Y, Gong S Q and Xu Z K 1999 *Acta Phys. Sin.* **48** 961 (in Chinese)

[2] Zhou X X and Li B W 2001 *Acta Phys. Sin.* **50** 1902 (in Chinese)

[3] Wu J H and Yan J M 2003 *Chin. Phys.* **12** 1390

[4] Li P C, Zhou X X, Dong C Z and Zhao S F 2004 *Acta Phys. Sin.* **53** 750 (in Chinese)

[5] Zheng Y H, Zeng Z N, Li R X and Xu Z Z 2007 *Acta Phys. Sin.* **56** 2243 (in Chinese)

[6] Zhang Y P, Zhang F S, Meng K L and Xiao G Q 2007 *Chin. Phys.* **16** 83

[7] Zhou Z Y and Yuan J M 2007 *Chin. Phys.* **16** 675

[8] Ge Y C 2005 *Chin. Phys. Lett.* **23** 2461

[9] Spielmann C and Burnett N H 1997 *Science* **278** 661

[10] Drescher M, Hentschel M, Kienberger R, Tempea G, Spielmann C, Reider G A, Corkum P B and Krausz F 2001 *Science* **291** 1923

[11] Hentschel M, Kienberger R, Spielmann C, Reider G A, Milosevic N, Brabec T, Corkum P B, Heinzmann U, Drescher M and Krausz F 2001 *Nature* **414** 509

[12] Drescher M, Hentschel M, Kienberger R, Uiberacker M, Yakovlev V, Scrinzi A, Westerwalbesloh T, Kleineberg U, Heinzmann U and Krausz F 2002 *Nature* **419** 803

[13] Kienberger R, Goulielmakies E, Uiberacker M, Baltuska A, Yakovlev V, Bammer F, Scrinzi A, Westerwalbesloh T, Kleineberg U, Heinzmann U, Drescher M and Krausz F 2004 *Nature* **427** 817

[14] Constant E, Taranukhin V D, Stolow A and Corkum P B 1997 *Phys. Rev.* A **56** 3870

[15] Dinu L C, Muller H G, Kazamias S, Mullot G, Augé F, Balcou P, Paul P M, Kovačev M, Breger P and Agostini P 2003 *Phys. Rev. Lett.* **91** 063901

[16] Bandrauk A D, Chelkowski S and Shon N H 2003 *Phys. Rev.* A **68** 041802(R)

[17] Itatani J, Quéré F, Yudin G L, Ivanov M Y, Krausz F and Corkum P B 2002 *Phys. Rev. Lett.* **88** 173903

[18] Kitzler M, Milosevic N, Scrinzi A, Krausz F and Brabec T 2002 *Phys. Rev. Lett.* **88** 173904

[19] Quéré F, Itatani J, Yudin G L and Corkum P B 2003 *Phys. Rev. Lett.* **90** 073902

[20] Mairesse Y and Quéré F 2005 *Phys. Rev.* A **71** 011401(R)

[21] Sansone G, Benedetti E, Calegari F, Vozzi C, Avaldi L, Flammini R, Poletto L, Villoresi P, Altucci C, Velotta R, Stagira S, Silvestri S D and Nisoli M 2006 *Science* **314** 443

[22] Quéré F, Mairesse Y and Itatani J 2005 *J. Mod. Opt.* **52** 339
V. S. Yakovlev, F. Bammer and A. Scrinzi 2005 *J. Mod. Opt.* **52** 395

[23] Ge Y C 2005 *Acta Phys. Sin.* **54** 2653 (in Chinese)

[24] Ge Y C, Li Y J and Kang K J 2005 *Acta Phys. Sin.* **54** 2669 (in Chinese)

[25] Ge Y C 2006 *Acta Phys. Sin.* **55** 3386 (in Chinese)

[26] Ge Y C 2006 *Chin. Phys.* **15** 2909

[27] Ge Y C 2006 *Phys. Rev.* A **74** 015803

[28] Lewenstein M, Balcou P, Ivanov M Y, LHuillier A and Corkum P B 1994 *Phys. Rev.* A **49** 2117

[29] Brabec T and Krausz F 2000 *Rev. Mod. Phys.* **72** 545

[30] Milosevic D B and Ehlotzky F 1998 *Phys. Rev.* A **58** 3124